Available online at www.sciencedirect.com

SciVerse ScienceDirect

Journal of the European Ceramic Society 32 (2012) 823–834

www.elsevier.com/locate/jeurceramsoc

Hot corrosion behaviors of gas tunnel type plasma sprayed $La_2Zr_2O_7$ thermal barrier coatings

Subramaniam Yugeswaran [a], Akira Kobayashi [a,*], P.V. Ananthapadmanabhan [b]

[a] *Joining & Welding Research Institute, Osaka University, 11-1 Mihogaoka, Ibaraki, Osaka 567-0047, Japan*
[b] *L & PT Division, Bhabha Atomic Research Centre, Mumbai 400085, India*

Received 8 July 2011; received in revised form 19 October 2011; accepted 29 October 2011
Available online 21 November 2011

Abstract

Gas tunnel type plasma sprayed free-standing $La_2Zr_2O_7$ coating specimens with a thickness of 300–400 μm were prepared under optimized operating conditions and were subjected to hot corrosion test in the presence of corrosive impurities such as V_2O_5, Na_2SO_4, and $Na_2SO_4 + V_2O_5$ mixtures (60:40 wt%) at two different temperatures for duration of 5 h, i.e. 1000 and 1350 K for V_2O_5 and $Na_2SO_4 + V_2O_5$ mixtures, 1200 and 1350 K for Na_2SO_4. For temperatures at 1350 K, the reaction mechanism of V_2O_5 and the mixture of $Na_2SO_4 + V_2O_5$ are similar and $LaVO_4$ is formed as the corrosive product, which leads to massive phase transformation from pyrochlore to tetragonal and monoclinic phases. Microstructural observations from planar reaction zone (PRZ) and melt infiltrated reaction zone (MIRZ) reveals that the present $La_2Zr_2O_7$ coating exhibits good hot corrosion resistance in V_2O_5 environment and moderate for the mixture of $Na_2SO_4 + V_2O_5$, but is worst in Na_2SO_4 environment.

Keywords: $La_2Zr_2O_7$; Thermal barrier coating; Gas tunnel type plasma; Hot corrosion; Surfaces; Microstructure

1. Introduction

Plasma-sprayed thermal barrier coatings (TBC) are traditionally applied to critical hot sections of the industrial gas turbines, particularly, turbine blades, vanes and combustion chambers in order to protect the hot sections from this high operating temperature and increase the component durability. Simultaneously, the need for enhancing the fuel efficiency has lead to increase in the operating temperatures of gas turbines year after year. Hence, the reliability of the most widely used TBC top coat composition, i.e. yttria stabilized zirconia (YSZ) coatings, has been weakened due to its phase transformation and sintering or densification behavior at higher operating temperatures and corrosive environments, which might result in disintegration of the coating.[1–4]

Therefore, development of new materials for TBC in order to address the challenges of the highly demanding operating environments is essential to fulfill the industrial requirements. Recently, it has been found that some very interesting properties are possessed by one composition, i.e. pyrochlore phase lanthanum zirconate ($La_2Zr_2O_7$). The results of the earlier works have shown that this material has excellent thermal stability, (which is stable up to its melting point: 2573 K), low thermal conductivity (1.56 $W\,m^{-1}\,K^{-1}$, compared to 2.12 $W\,m^{-1}\,K^{-1}$ for YSZ[4]), low sintering rate, and thus becomes a very promising candidate for new TBC material.[5–7] However, relatively low thermal expansion coefficient of about $9 \times 10^{-6}\,K^{-1}$ compared to YSZ with 10–11 $\times\ 10^{-6}\,K^{-1}$ leads to higher thermal stresses due to thermal expansion mismatch between the coating interfaces and causes severe damage in the coating system.[8,9]

Vassen et al.[10] studied the thermo-physical properties of $La_2Zr_2O_7$ material and successfully produced a coating through APS technique. Observation from their results clearly underlines that $La_2Zr_2O_7$ has good potential as a new material for advanced TBCs, even though it has lower Young's modulus and thermal expansion than that of YSZ. Furthermore, their results proved that the thermal conductivity of $La_2Zr_2O_7$ which is approximately 20% lower than that of YSZ is favorable at elevated temperatures, and also shows excellent thermal stability. Subsequently, they developed YSZ/$La_2Zr_2O_7$ multilayer layer coating systems in order to enhance the cyclic life time of the coating under high operating temperatures.[11,12] Likewise, Chen

* Corresponding author. Tel.: +81 6 6879 8694; fax: +81 6 6879 8694.
E-mail address: kobayasi@jwri.osaka-u.ac.jp (A. Kobayashi).

0955-2219/$ – see front matter © 2011 Elsevier Ltd. All rights reserved.
doi:10.1016/j.jeurceramsoc.2011.10.049

et al.[13] stated that the graded YSZ/$La_2Zr_2O_7$ coating offers admirable thermal shock resistance in comparison to that of its duplex and single layer coatings. Actually they have prepared six-layered YSZ/$La_2Zr_2O_7$ bicomponent graded coatings through plasma spraying. These authors also prepared structured $La_2Zr_2O_7$ coatings through plasma spraying and studied their thermophysical properties. Astonishingly, the coating exhibited minimum thermal conductivity, i.e. 0.73 W m^{-1} K^{-1}, which was about 50% lower than previously reported results of conventional microstructure coatings.[14]

It should be noted that the hot corrosion mechanism of the TBC material against different kinds of corrosive environment is also one of the imperative factors that must be taken into account along with other factors such as thermal conductivity, phase stability, thermal expansion coefficient and mechanical properties of the TBC material while searching for new TBC materials or while validating the existing one as a promising TBC material. Hence the understanding of hot corrosion reaction mechanisms of the $La_2Zr_2O_7$ against different kinds of corrosive ashes at elevated temperatures is a must for categorizing or widening the application of $La_2Zr_2O_7$. Since in most of the cases, the TBCs are subjected to face low-quality fuels during operation, the impurities in the highly contaminated fuel can combine to form molten salts, such as sodium sulfate and vanadium compounds and deposit on the coating surface in the combustion environment, giving rise to hot corrosion problems.[15]

There are only a few earlier reports[16,17] that exemplify the hot corrosion behavior of plasma sprayed $La_2Zr_2O_7$ coatings against V_2O_5, Na_2SO_4 and V_2O_5, $Na_2SO_4 + V_2O_5$ corrosive environments at elevated temperatures and different time durations, but they are insufficient when compared to the reports of conventional YSZ coating hot corrosion results.[18–20] Hence in this paper, further examinations of the hot corrosion behavior of plasma sprayed $La_2Zr_2O_7$ coatings against V_2O_5, Na_2SO_4, and $Na_2SO_4 + V_2O_5$ mixtures (60:40 wt%) corrosive salts at elevated temperatures was conducted and the results are discussed with regard to corrosive product formation and microstructural changes. For this purpose, free-standing $La_2Zr_2O_7$ coating specimens with thickness of around 300–400 μm were prepared by using gas tunnel type plasma spray torch under optimized operating conditions. Superiority, unique features of gas tunnel type plasma spraying and the influence of its processing parameters on the ceramic coating formation are well reported in previous publications.[21–23]

2. Experimental procedure

Fig. 1 shows a schematic of the gas tunnel type plasma spraying torch and a photographic image of its high energy density plasma jet, which was used for producing $La_2Zr_2O_7$ coatings required for this study. For this purpose, $La_2Zr_2O_7$ powder was commercially procured and its typical surface morphology is shown in Fig. 2. The SEM morphology reveals that the feedstock grains are irregular in nature with average size range of 10–40 μm. Argon gas was used as carrier gas with a flow rate of 5 lpm to carry the $La_2Zr_2O_7$ powder from the feeder at the rate of

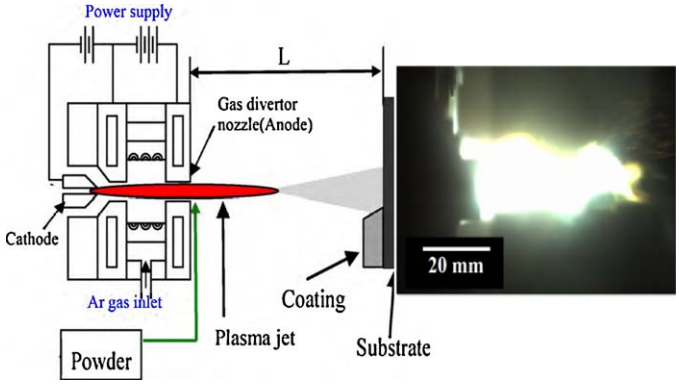

Fig. 1. Schematic of gas tunnel type plasma spraying torch and the image of dense plasma jet.

15 g/min to form a coating on SUS304 substrate under a spraying current of 350 A with a total (primary and vortex) gas argon flow rate of 180 lpm. The powder was fed at the nozzle exit and the torch to base (substrate) distance was 50 mm. The torch operating parameters used in the present coating were selected in order to get dense coating with thickness of around 300–400 μm and also taking caution that there is minimal deviation from the initial stoichiometric ratio. The optimum spraying parameters for $La_2Zr_2O_7$ coatings in gas tunnel type plasma spray torch were identified based on numerous trial experiments. After spraying, free-standing $La_2Zr_2O_7$ coating specimens were obtained by a simple heat treatment in an open atmosphere electrical furnace. For this purpose, $La_2Zr_2O_7$ feedstock was sprayed on smooth surface of SS-304 substrate. After that the coated substrates were cut into samples of dimension 2 cm × 2 cm and heated in electrical furnace up to 1000 °C for 3 h. This temperature was sufficient to peel out the ceramic coating from the substrate.

Hot corrosion testing was performed to study the reaction mechanisms of $La_2Zr_2O_7$ coating against V_2O_5, Na_2SO_4 and $Na_2SO_4 + V_2O_5$ mixture at elevated temperatures. For this purpose, coating specimens with dimension of 2 cm × 2 cm were sectioned from the as-sprayed free-standing $La_2Zr_2O_7$ coatings. Then, fine grained corrosive salts such as V_2O_5 and $Na_2SO_4 + V_2O_5$ mixture at 60:40 wt% were individually spread

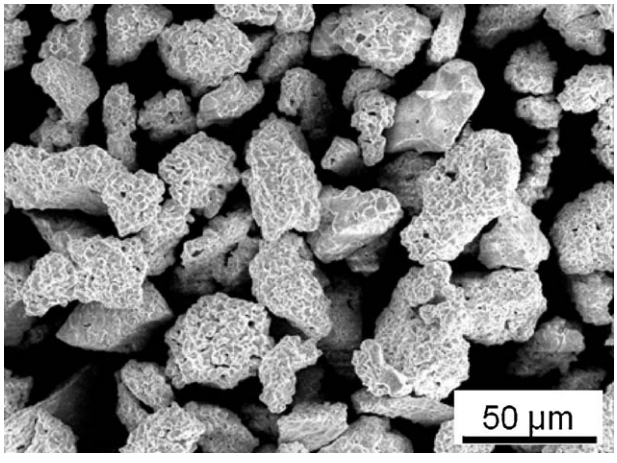

Fig. 2. SEM image of $La_2Zr_2O_7$ feedstock powder.

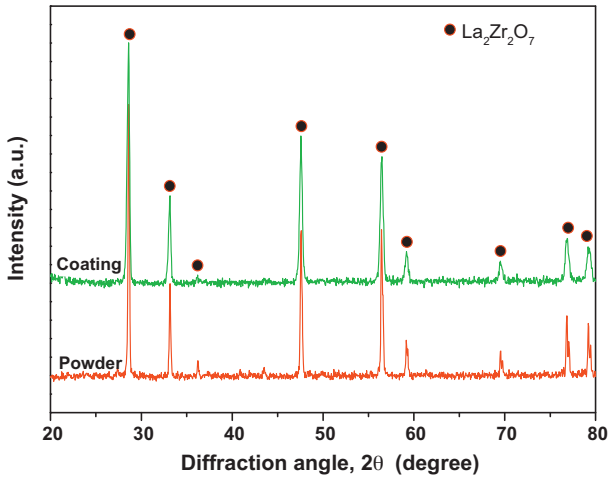

Fig. 3. XRD pattern of $La_2Zr_2O_7$ powder and sprayed coating (at 350 A).

over the as-sprayed free-standing coating surfaces by using a very fine glass rod at a concentration of 20 mg/cm^2 and then the coating was subjected to isothermal heat treatments at temperatures of 1000 and 1350 K for 5 h duration in air. For hot corrosion experiments with Na_2SO_4, the salt was applied at higher concentrations such as 40 mg/cm^2 and then the coating was subjected to isothermal heat treatments at temperatures of 1200 and 1350 K for 5 h duration because of the less reactive nature and relatively high melting point of Na_2SO_4. The reactions with each compound were isolated, thereby eliminating mixed interactions and combined effects. For all the experiments, the sample heating and cooling rates were kept at 10 °C/min and 5 °C/min respectively. The concentrations of the corrosive salts chosen during this study are only to examine the hot corrosion mechanisms of the coating, not for actual condition of TBC while at operation. Finally, the specimens were removed from the furnace after they reached room temperature and then were subjected to characterization.

"X-ray diffraction (XRD) studies were performed on the hot corrosion-tested samples to examine the resulting corrosion products and the phase transformations. This was performed by using a JEOL JDX-3530M diffractometer with Cu-Kα radiation source at a voltage of 40 kV and current of 40 mA. The analysis was performed at a scan speed of 5°/min for values of 2θ between 10° and 90°. Surface and cross-sectional

Table 1
Chemical compositions and lattice parameter of $La_2Zr_2O_7$ powder and coating.

Samples	Chemical compositions		Lattice parameter (a)
	La (wt%)	Zr (wt%)	(Å)
$La_2Zr_2O_7$ powder	46.58	33.60	10.824
$La_2Zr_2O_7$ coating	41.95	36.28	10.884
Theoretical value[25]	48.6	31.9	

microstructural analysis was carried out to examine corrosive product formation and degradation reaction mechanisms using an ERA8800 field-emission scanning electron microscope (FE-SEM) equipped with an energy dispersive spectrometer (XEDS). For the microstructural characterization, corrosive specimens were embedded in epoxy resin and were metallographically prepared. Information on the phase and the microstructure of the initial feedstock and the as-sprayed free-standing coatings was also obtained using the same equipments.

3. Results and discussion

Fig. 3 shows the XRD patterns of the $La_2Zr_2O_7$ powder and its plasma sprayed coating. The XRD pattern revealed that the pyrochlore phase of $La_2Zr_2O_7$ was stable even in the coating obtained at higher plasma current (350 A) under the optimized plasma torch spraying conditions. The main feature of this XRD investigation is that the obtained peaks belonging to the pyrochlore structure shift slightly towards smaller 2θ value and cause larger lattice parameter than that of the initial powder. Furthermore, the stoichiometric ratios of ZrO_2/La_2O_3 varied significantly in the coating compared to the ratio in the initial powder, which was confirmed by the EDX analysis and is shown in Table 1. This deviation can be attributed to the in-flight loss of La_2O_3 in $La_2Zr_2O_7$ during the plasma spray process.[24,25] However, the above variation does not affect the pyrochlore structure because of the considerable solubility range of $La_2Zr_2O_7$ from 53.6 wt% La_2O_3 and 46.4 wt% ZrO_2 to 60.4 wt% La_2O_3 and 39.6 wt% ZrO_2 whereby the crystalline structure and properties remain unaffected.[24] In general, ZrO_2 is thermally more stable than La_2O_3 in pyrochlore structure[26] and this will cause different

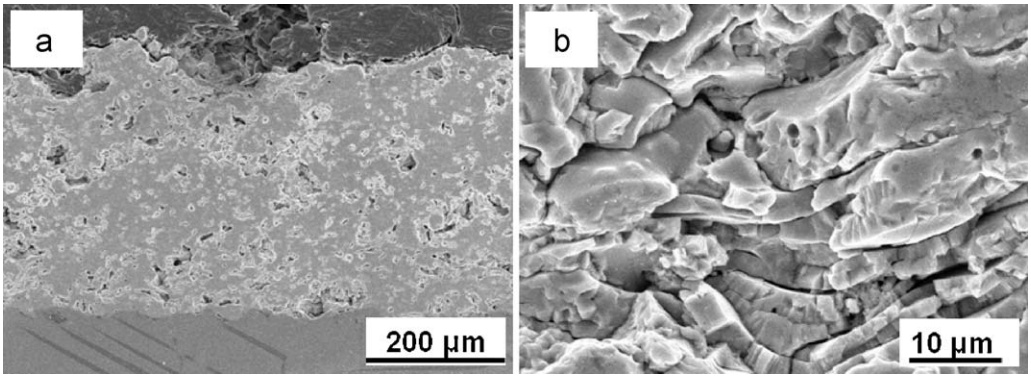

Fig. 4. Cross-section SEM images of $La_2Zr_2O_7$ coatings (a) and its splat orientation (b).

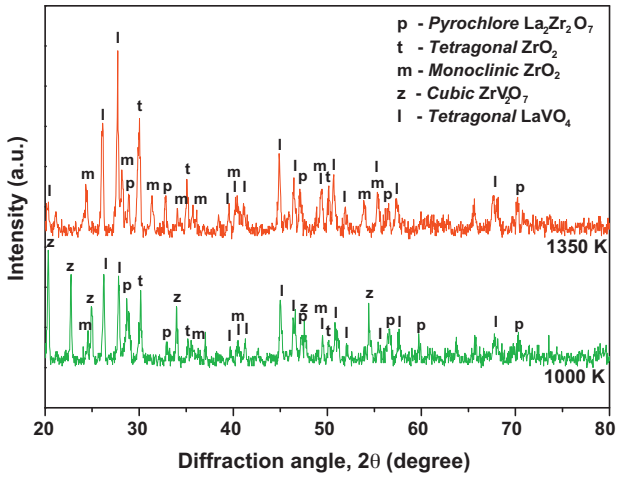

Fig. 5. XRD patterns of $La_2Zr_2O_7$ coating after hot corrosion test against V_2O_5 at 1000 and 1350 K for a duration of 5 h.

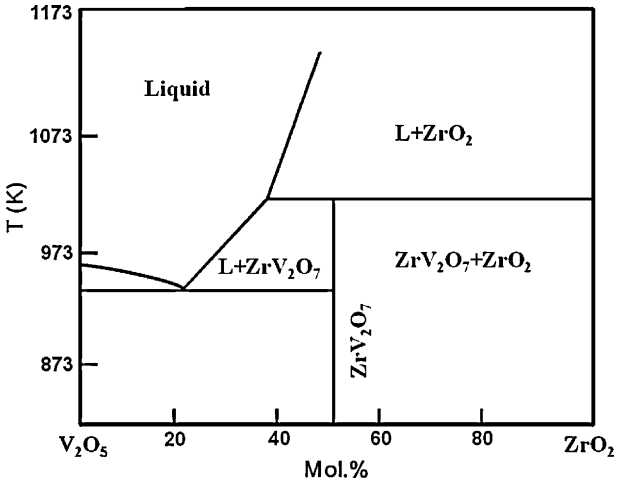

Fig. 6. ZrO_2–V_2O_5 phase diagram.[28]

evaporation rates of the components leading to stoichiometric change while spraying in high temperature plasma jet.

The typical cross-sectional micrographs of the gas tunnel type plasma sprayed $La_2Zr_2O_7$ free standing coatings and its higher magnification are shown in Fig. 4. The thickness of all the coatings is around 300–400 μm and the distribution of porosity along the cross section was measured at four different areas by image analysis and is around 9–11%. The coatings present a porous and lamellar structure which is a unique characteristic for this kind of spraying, but it could be controlled by optimizing the spraying conditions. Herein, the splats are separated by interlamellar pores resulting from rapid solidification of the lamellae. Sporadically, fine voids also appear nearby the un-melted particles along with few cracks due to thermal stresses and tensile quenching relaxation stresses. Favorably, the presence of cracks also increases the strain tolerance and enhances the thermal shock resistance of TBCs in service.

3.1. Hot corrosion of $La_2Zr_2O_7$ coating against V_2O_5

In this investigation, hot corrosion studies were performed at a temperature of 1000 K and also 1350 K. Fig. 5 shows the XRD patterns obtained from the reaction zone of V_2O_5 coated $La_2Zr_2O_7$ heat treated at 1000 K and 1350 K for a duration of 5 h. The reactions at elevated temperatures lead to the formation of new phases such as cubic phase zirconium pyrovanadate (ZrV_2O_7), tetragonal phase lanthanum vanadate ($LaVO_4$), tetragonal and monoclinic phases of zirconia (ZrO_2) along with pyrochlore phase of $La_2Zr_2O_7$. However, the presence of corrosion products and the intensities of the transforming phases drastically differ between the two hot corrosion temperatures. At 1000 K, $La_2Zr_2O_7$ was found to react with molten V_2O_5 and form ZrV_2O_7 as the major corrosion product along with substantial amount of $LaVO_4$. The formation of the corrosive products resulted in the disruptive $La_2Zr_2O_7$ phase transformation partially from pyrochlore to tetragonal and monoclinic phase ZrO_2. The formation of ZrV_2O_7 should enrich La_2O_3 in $La_2Zr_2O_7$ due to depletion of ZrO_2 during reaction with V_2O_5, and promote the formation of $LaVO_4$ from the residues of La_2O_3 and V_2O_5. The reactions involved in the formation of ZrV_2O_7 are slow which has been clearly stated in earlier reports and literature,[27] but the results of the studies by Chen et al.[15] show that this is certainly not the case for reaction temperatures below 1000 K, where the V_2O_5 and the YSZ coating react to form ZrV_2O_7 within minutes of reaching 973 K. A possible reaction that could have produced these phases can be written as:

$$La_2Zr_2O_7(s) + 3\,V_2O_5(l) \rightarrow 2ZrV_2O_7(s) + 2LaVO_4(s) \quad (\leq 1000\,K) \tag{1}$$

The interpretation of the ZrO_2–V_2O_5 phase diagram which is shown in Fig. 6 might be useful to explain the results of the XRD pattern. According to the phase diagram, pure V_2O_5 liquid in contact with ZrO_2 at 973 K can dissolve approximately 30 mol.% zirconia in solution before the first solid reaction product (ZrV_2O_7) can form. For compositions of 50 mol.% V_2O_5/50 mol.% ZrO_2, only ZrV_2O_7 should be present. Hence, ZrV_2O_7 should be the first reaction product formed from the reaction of ZrO_2 and V_2O_5, followed by precipitation of m-ZrO_2 as the vanadium oxide concentration continues to diminish. Similarly at this stage in the La_2O_3–V_2O_5 system, pure liquid V_2O_5 will dissolve significant amounts of La_2O_3 and produce $LaVO_4$ as a minimally soluble precipitate which is highly stable up to 2083 K.[29]

Meanwhile, the XRD pattern obtained from the reaction zone of V_2O_5 coated $La_2Zr_2O_7$ which was heat treated at 1350 K for 5 h clearly shows that it is different from that obtained at 1000 K. Only $LaVO_4$ seems to be the major corrosion product along with considerable amount of tetragonal and monoclinic phases of ZrO_2. The other corrosion product phase ZrV_2O_7 was absent at this temperature due to the thermal decomposition of ZrV_2O_7 which starts at 1020 K. At temperatures above 1020 K, the molten ZrV_2O_7 decomposes into monoclinic phase ZrO_2 and a mixture of monoclinic phase ZrO_2 and liquid V_2O_5. Then the molten V_2O_5 from ZrV_2O_7 reacts with $La_2Zr_2O_7$ to form ZrV_2O_7 and $LaVO_4$, as shown in Eq. (1). Concomitantly,

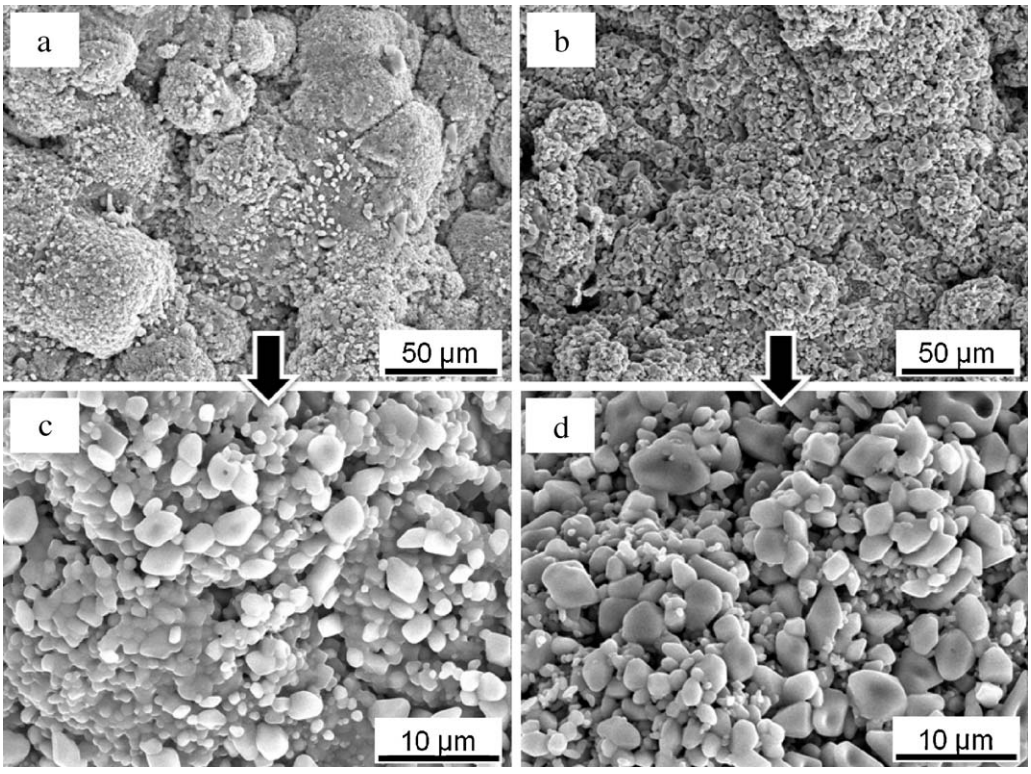

Fig. 7. Typical surface micrographs of $La_2Zr_2O_7$ coating after the hot corrosion test against V_2O_5 for 5 h at: (a) and (c) 1000 K; (b) and (d) 1350 K.

ZrV_2O_7 melts and decomposes into monoclinic ZrO_2 and a mixture of monoclinic ZrO_2 and liquid V_2O_5. This process is repeated until V_2O_5 is completely depleted and $LaVO_4$ and monoclinic ZrO_2 are formed as the final products. However, the excess La_2O_3 in partially dissociated pyrochlore phase $La_2Zr_2O_7$ can serve as a stabilizing agent up to its threshold limit and predominantly stabilize the ZrO_2 in tetragonal phase. This reduces the amount of monoclinic phase ZrO_2 and consequently the tetragonal ZrO_2 becomes the predominant phase rather than monoclinic phase in the XRD pattern of the present study. The reaction mechanism at temperatures above 1020 K is given by the following chemical equation:

$$La_2Zr_2O_7(s) + V_2O_5(l) \rightarrow 2LaVO_4(s) + 2ZrO_2(s) \quad (\geq 1020\,K) \qquad (2)$$

Typical surface micrographs of $La_2Zr_2O_7$ coatings after the hot corrosion test against V_2O_5 for 5 h at 1000 and 1350 K are shown in Fig. 7. In both cases, the reaction of the molten V_2O_5 on the $La_2Zr_2O_7$ coating resulted in the conversion of the typical plasma sprayed splat-lamellae structure into clusters of fine equiaxed particles. Moreover, the magnified images of the corroded surfaces from Fig. 7(c) and (d) revealed that the microstructure of the corroded surfaces seemed to be slightly differing from each other. The clusters of fine equiaxed particles of the corrosion products such as $LaVO_4$, ZrV_2O_7 and ZrO_2 on the surface heat-treated at 1000 K were well bounded with each other, whereas the above equiaxed particles are well isolated from each other on the surface heat-treated at 1350 K, which is confirmed by EDX spectrum shown in Fig. 8. Previous XRD results showed that one of the major hot corrosion products, ZrV_2O_7 is absent on the coating surface heat treated at 1350 K due to thermal decomposition of ZrV_2O_7 which starts at 1020 K. Hence, the correlation between the XRD and microstructure results confirms that the presence of ZrV_2O_7 in the samples heat treated at 1000 K is the main reason for the

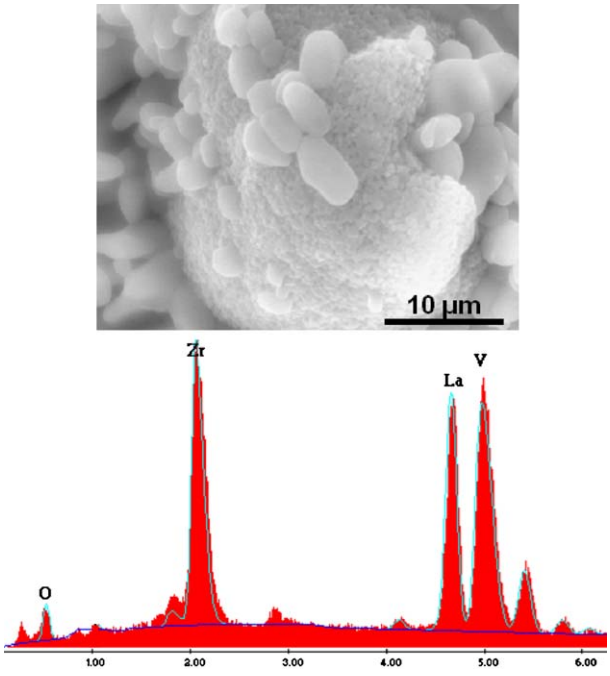

Fig. 8. EDX spectrum of V_2O_5 reacted $La_2Zr_2O_7$ coating zone at 1350 K.

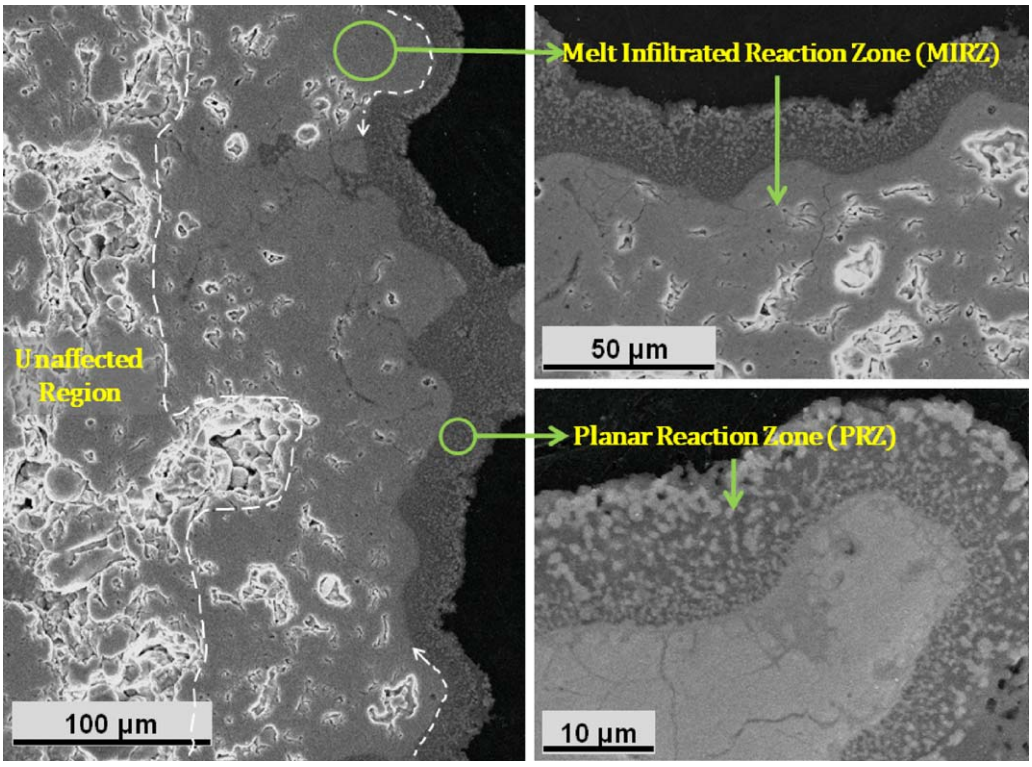

Fig. 9. Cross-sectional micrographs of $La_2Zr_2O_7$ coating zone after corroded by V_2O_5 at 1000 K for 5 h.

differences in the microstructural features occurring in the surfaces of $La_2Zr_2O_7$ coatings after hot corrosion reaction of V_2O_5 at 1000 and 1350 K.

Furthermore, the interconnected network of interlamellar pores and intralamellar cracks of the plasma sprayed $La_2Zr_2O_7$ coating, affords the penetration of molten V_2O_5 liquids within the coating. Generally, plasma sprayed coating is built-up by lamellae with pores and cracks between them. Most of the interlamellar pores are oriented parallel to the coating surface and similarly intralamellar cracks are oriented along the boundaries of columnar grains, and interlamellar pores

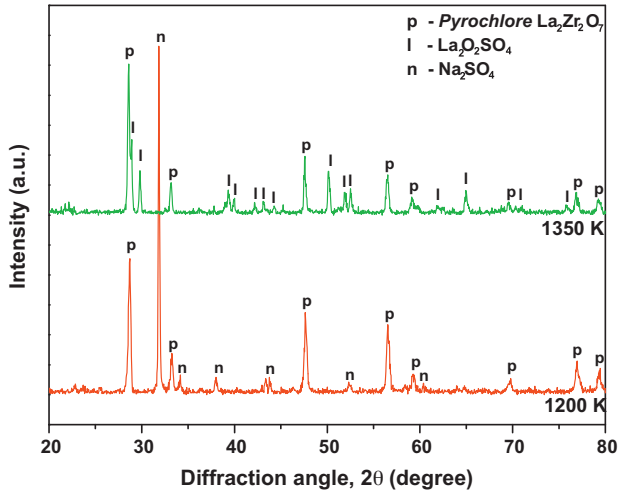

Fig. 10. XRD patterns of $La_2Zr_2O_7$ coating after hot corrosion test against Na_2SO_4 at 1200 and 1350 K for a duration of 5 h.

between lamellae. Hence, the penetration of molten V_2O_5 into the coating microstructure through the pore network can produce two different kinds of microstructures such as the planar reaction zone (PRZ) and melt infiltrated reaction zone (MIRZ). Fig. 9 shows the different morphology of the $La_2Zr_2O_7$ coating cross-section after corrosion by molten V_2O_5 at 1000 K for a duration of 5 h. During the reaction, the lamellae near the surface of the coating completely dissolve in the molten V_2O_5 liquid and precipitate out as clusters of sub-micron equiaxed particles such as $LaVO_4$, ZrV_2O_7 and or ZrO_2. Moreover, melting of V_2O_5 and transformation of lamellae to particles were completed in this region. This fully reacted region is called the planar reaction zone (PRZ) which appears as a porous layer along with slackly connected corroded particles. The depth of the PRZ varied from 15 to 25 μm throughout the reaction zone with respect to $La_2Zr_2O_7$ coating surface morphology. Earlier, Chen et al.[30] have described the comprehensive mechanism of PRZ and MIRZ formation in plasma sprayed YSZ thermal barrier coating against V_2O_5 corrosive environment at elevated temperatures.

Below the PRZ, the coating microstructure seems to be dense with preserved lamellar structure and a thickness ranging from 150 to 200 μm. This dense region is called the melt infiltrated reaction zone (MIRZ), which is formed by melt infiltration of the molten V_2O_5 into the coating through the cracks and pores. Conversely, some part of the MIRZ was filled with equiaxed corroded particles as in PRZ, prior to which they were macro pores in the as-sprayed coating. This observation might act as an evidence of the pore network and its vital role in the coating microstructure evolution during the hot corrosion.

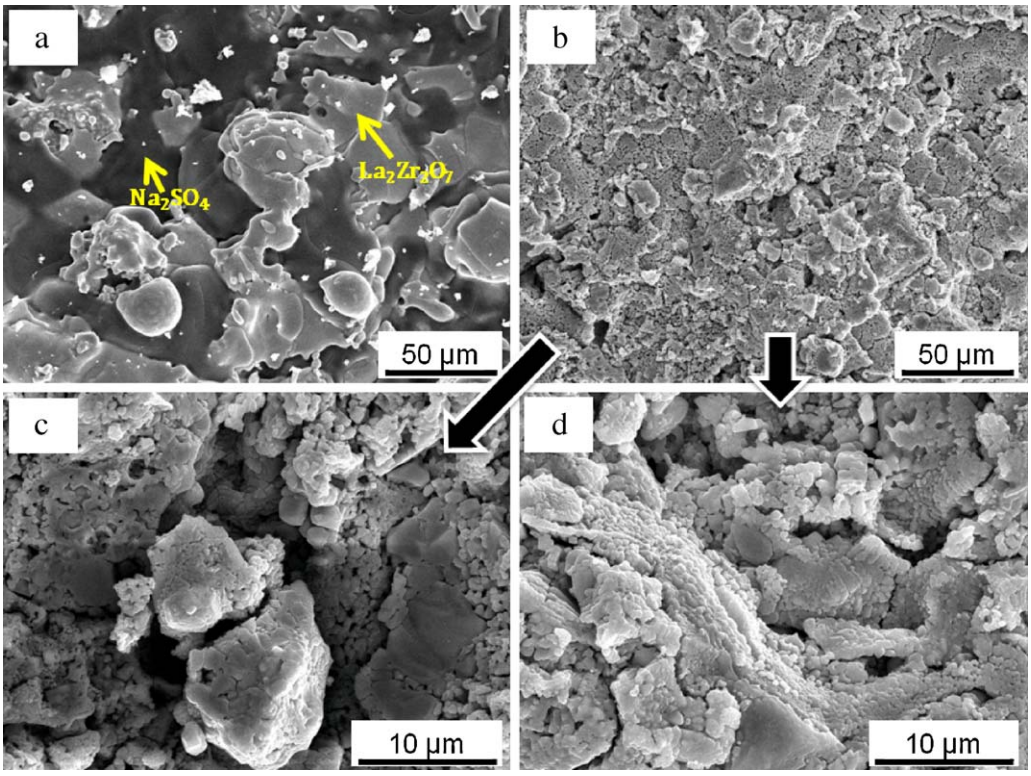

Fig. 11. Typical surface micrographs of $La_2Zr_2O_7$ coating after hot corrosion test against Na_2SO_4 for 5 h at: (a) 1200 K; (b)–(d) 1350 K.

However, beyond the region of MIRZ, the $La_2Zr_2O_7$ coating microstructure has remained unaffected nearly around 100 μm, which is clearly observed from Fig. 9. Thus, the unaffected regions have a unique plasma sprayed microstructure, i.e. with a lamellar microstructure along with residual pores and microcracks. The thickness of the unaffected regions plays an essential role in determining the life time of TBC during operation in hot corrosion environments.

3.2. Hot corrosion of $La_2Zr_2O_7$ coating against Na_2SO_4

Na_2SO_4 melts at 1157 K, so the hot corrosion studies of $La_2Zr_2O_7$ specimens were conducted at temperatures of 1200 K and 1350 K. For all the experiments, the sample heating and cooling rates were kept at 10 °C/min and 5 °C/min respectively. XRD results obtained from the reaction zone of Na_2SO_4 coated $La_2Zr_2O_7$ heat treated at 1200 K and 1350 K for a duration of 5 h are shown in Fig. 10. The reaction zone pattern at 1200 K for 5 h revealed the presence of only the initial phases of $La_2Zr_2O_7$ and Na_2SO_4 with no evidence of phase transformation or reaction between $La_2Zr_2O_7$ and Na_2SO_4. At this temperature, Na_2SO_4 gets melted and the molten Na_2SO_4 infiltrates through the open pores and interlamellar gaps of $La_2Zr_2O_7$ coating and after that the molten salt was found to have crystallized in the cracks and pores of the coating during cooling. X-ray diffraction results did not reveal the presence of any new phase confirming that there was no reaction between $La_2Zr_2O_7$ and Na_2SO_4.

The pattern of the 1350 K heat treated Na_2SO_4 coated $La_2Zr_2O_7$ reaction zone appears with initial phases of $La_2Zr_2O_7$ along with lanthanum oxide sulfate ($La_2O_2SO_4$) as the corrosion product. At this temperature, the molten Na_2SO_4 reacts with La_2O_3 in $La_2Zr_2O_7$ and forms $La_2O_2SO_4$ by the following possible reaction mechanism which can be expressed as:

$$2La_2Zr_2O_7(s) + 6Na_2SO_4(l) \rightarrow La_2O_2SO_4(s) + La_2(SO_4)_3(s) + 4ZrO_2(s) + 2SO_3(g) + 6Na_2O(l) \quad (at 1350\,K) \quad (3)$$

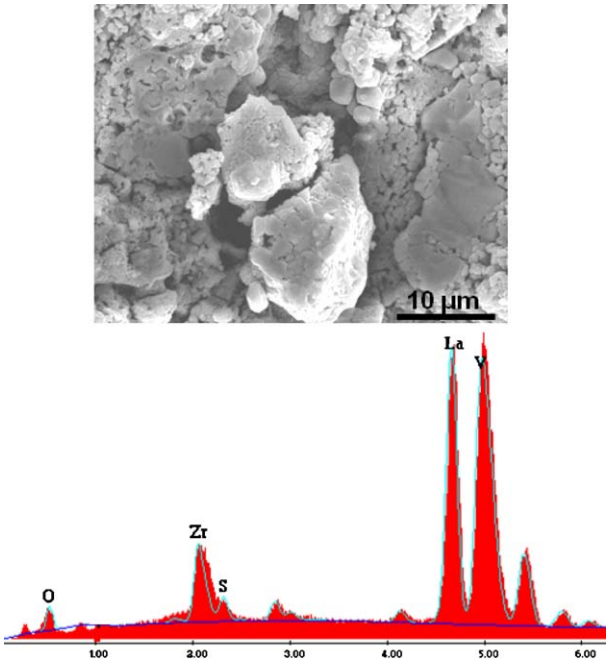

Fig. 12. EDX spectrum of Na_2SO_4 reacted $La_2Zr_2O_7$ coating zone at 1350 K.

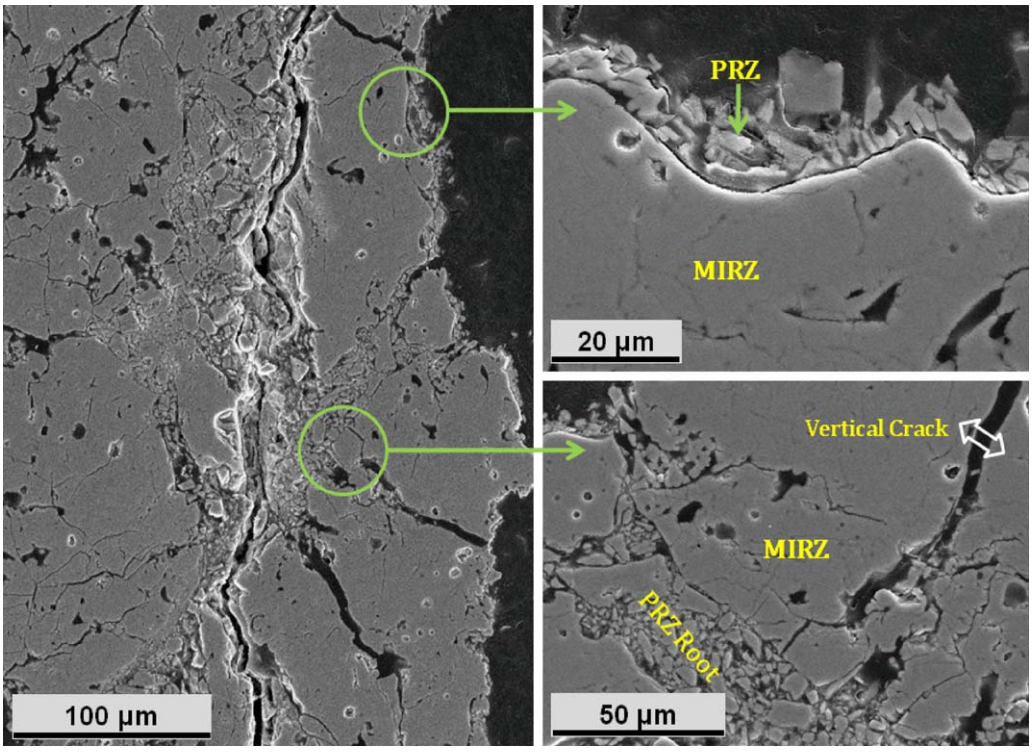

Fig. 13. Cross-sectional micrographs of $La_2Zr_2O_7$ coating after hot corrosion reaction of Na_2SO_4 at 1350 K for 5 h.

The above chemical reaction also indicates the formation of lanthanum sulfate ($La_2(SO_4)_3$) as a possible corrosion product in the Na_2SO_4 - $La_2Zr_2O_7$ reaction zone, but at this study temperature it is decomposing via an oxysulfate. Previous researchers observed that the initial decomposition temperatures for lanthanum sulfate ($La_2(SO_4)_3$) ranges from 973 K to 1113 K[31] and 1373 K for the oxysulfate.[32] These oxysulfate crystal forms increased in concentration with increasing temperature and became the dominant species at 1173 K. Hence, in the present study at 1350 K, lanthanum oxide sulfate, $La_2O_2SO_4$ is the possible corrosion product existing in the Na_2SO_4 reacted zone. This observation is consistent with the results obtained by Marple et al.,[16] where they have prepared $La_2Zr_2O_7$ coating through conventional plasma spraying technique and studied its hot corrosion resistance behavior against vanadium or sulfur compounds at elevated temperatures and exposure time. Furthermore, these results are compared with 8 wt.% yttria-stabilized zirconia coating hot corrosion results.

Typical surface micrographs of $La_2Zr_2O_7$ coating after hot corrosion testing against Na_2SO_4 at 1200 K and 1350 K for 5 h are shown in Fig. 11. The melting temperature of Na_2SO_4 is 1157 K, thus at this study temperature, i.e. 1200 K, it gets completely melted and the molten Na_2SO_4 disperses over the $La_2Zr_2O_7$ coating splat surfaces and gets crystallized during solidification. There is no significant reaction which occurs at this temperature, as was confirmed from the XRD result. Hence, the observed microstructure from Fig. 11(a) appears as sprayed coating splats with Na_2SO_4 phase intermingled or dispersed in it. On the contrary, the reaction of molten Na_2SO_4 on $La_2Zr_2O_7$ coating at 1350 K shown with different levels of magnification in Fig. 11(b)–(d) clearly indicates that the coating has experienced severe microstructural changes; the lamellar microstructure of $La_2Zr_2O_7$ coating turned into cohesive clusters of equiaxed grains. These grains are precipitates of $La_2Zr_2O_7$ and $La_2O_2SO_4$ which has been already confirmed from the XRD results as shown in Fig. 10 and EDX spectrum in Fig. 12.

Further comprehensive information on the microstructural changes can be obtained by observing the micrographs presented in Fig. 13, which shows a cross-sectional view of the Na_2SO_4 reacted $La_2Zr_2O_7$ coating zone at 1350 K with some magnified areas. The overall microstructure of the corroded coating seems to be almost intact, but it has been well distinguishable through different kind of microstructures such as PRZ and MIRZ, which are mentioned previously. Concurrently, the overall microstructure of the coating after Na_2SO_4 reaction drastically differed when compared to the V_2O_5 reacted $La_2Zr_2O_7$ coating microstructure. Formation of a number of vertical cracks and the deep penetration of PRZ through MIRZ, which formulate the complex microstructure are primarily responsible for this deviation. Most part of the coating was affected by hot corrosion reaction and experienced complete microstructural changes. Furthermore, formation of large crack (parallel to the coating surface) on the corroded coating surface is due to the chemical reaction, which weakens the inter-lamellar binding and the coating–substrate interface.

According to Eq. (3), formation of lanthanum sulfate is the major intermediate corrosive product after hot corrosion reaction of Na_2SO_4 on $La_2Zr_2O_7$ coating, but it decomposes above 973 K. Though, decomposition occurs at the phase boundary between the undecomposed sulfate and the oxide product, where the boundary proceeds regularly from the surface towards the interior, a phenomena analogous to the sharp interface shrinking

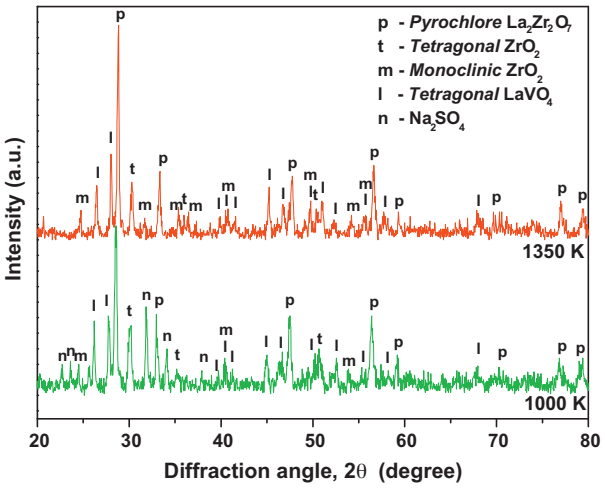

Fig. 14. XRD patterns of $La_2Zr_2O_7$ coating after hot corrosion test against $Na_2SO_4 + V_2O_5$ mixture (60:40, wt%) at 1000 and 1350 K for a duration of 5 h.

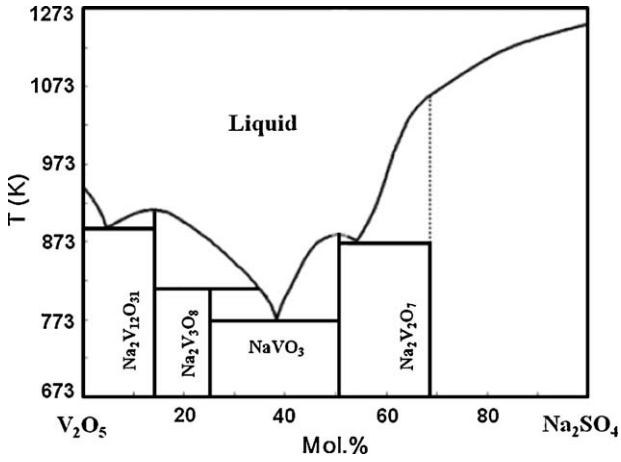

Fig. 15. V_2O_5–Na_2SO_4 phase diagram.[28]

core models, which may lead to drastic changes in the coating microstructure.[33,34] Results from the microstructural observations reveal that the $La_2Zr_2O_7$ coating is an unsuitable TBC material in Na_2SO_4 hot corrosion environment; as it may reduce the life time of TBC system.

3.3. Hot corrosion of $La_2Zr_2O_7$ coating against $Na_2SO_4 + V_2O_5$ mixture (60:40 wt%)

The previous results confirm that Na_2SO_4 does not react with $La_2Zr_2O_7$ up to around 1200 K due to its melting point (1157 K). Simultaneously, addition of V_2O_5 into Na_2SO_4 can entirely change the reaction mechanism and produce corrosive products even at temperatures below the melting point of Na_2SO_4. The XRD pattern of hot corrosion reaction of $Na_2SO_4 + V_2O_5$ mixture (60:40 wt%) on $La_2Zr_2O_7$ coating at 1000 and 1350 K for a duration of 5 h is shown in Fig. 14. In both the 1000 and 1350 K patterns, $LaVO_4$ is the only corrosive product formed along with consequent phase transformation from pyrochlore to tetragonal and monoclinic phases as previously mentioned in the corrosion reaction of V_2O_5 on $La_2Zr_2O_7$.

According to the Na_2SO_4–V_2O_5 phase system (Fig. 15), from 25 to 50 mol% of V_2O_5 i.e. 56 wt% in Na_2SO_4 mixture gives

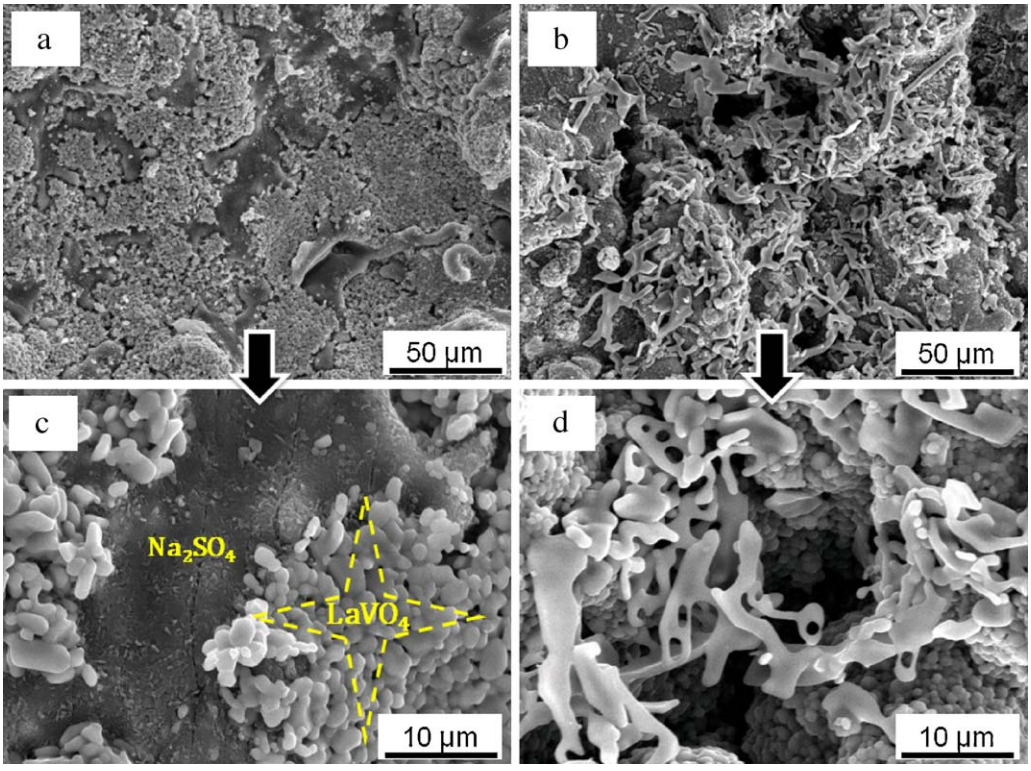

Fig. 16. Typical surface micrographs of $Na_2SO_4 + V_2O_5$ mixture (60:40, wt%) reacted $La_2Zr_2O_7$ coating zone heat treated for 5 h at: (a) and (c) 1000 K; (b) and (d) 1350 K.

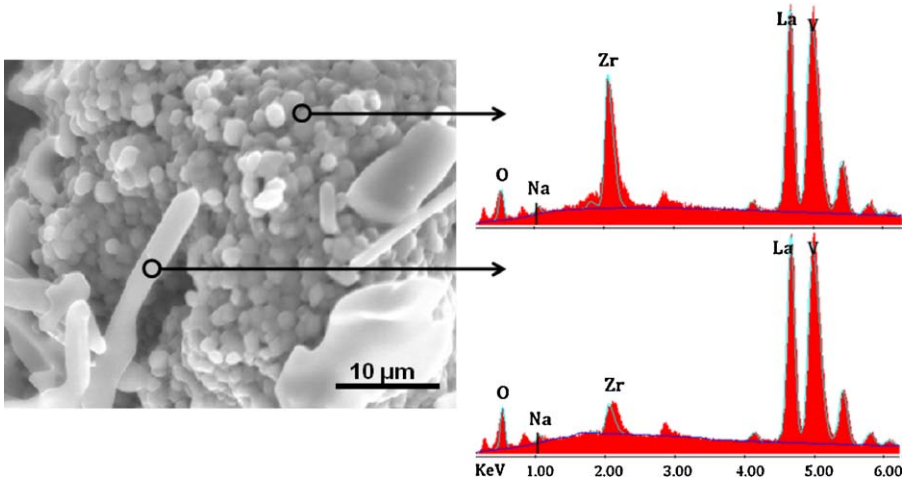

Fig. 17. EDX spectrums of $Na_2SO_4 + V_2O_5$ mixture reacted $La_2Zr_2O_7$ coating zone at 1350 K.

sodium metavanadate ($NaVO_3$) as the major reaction product for a temperature range from 773 to 883 K rather than other possible products such as NaV_3O_8 or $Na_4V_2O_7$.[35] Hence, the weight ratio taken in the present studies may also give $NaVO_3$ as the only reaction product. Consequently, the molten $NaVO_3$ continues to react with $La_2Zr_2O_7$ to form $LaVO_4$ as the final corrosion product in the interface between the top $Na_2SO_4 + V_2O_5$ layer and $La_2Zr_2O_7$ coating. The possible reaction mechanism is given by the following chemical equations:

$$Na_2SO_4(l) + V_2O_5(l) \rightarrow 2NaVO_3(l) + SO_3(g) \quad (4)$$

$$2NaVO_3(l) + La_2Zr_2O_7(s) \rightarrow 2LaVO_4(s) + 2ZrO_2(s) + Na_2O(l) \quad (5)$$

Moreover, minimal amount of Na_2SO_4 peaks appear in the pattern of 1000 K reaction XRD due to inappropriate mixing of V_2O_5 and consequent failure to melt, but the above crisis has entirely disappeared in 1350 K pattern. Concurrently, the phase transformations from pyrochlore to tetragonal and monoclinic phase ZrO_2 due to the depletion of La_2O_3 from $La_2Zr_2O_7$ did not significantly differ in both the patterns. Hence, the above results show that the formation of corrosive products from the reaction of Na_2SO_4–V_2O_5 (60:40 wt%) mixture and $La_2Zr_2O_7$ does not depend on its operating temperature when it is above the formation temperature of $NaVO_3$, i.e.773 K.

Typical surface micrographs depicting the reaction of 60:40 wt% of $Na_2SO_4 + V_2O_5$ mixture on $La_2Zr_2O_7$ coating zone at 1000 and 1350 K are shown in Fig. 16. At 1000 K, the surface combines with clusters of equiaxed corrosive grains and the layer of un-reacted Na_2SO_4 or some other residues of Na. Typical plasma sprayed lamella structure was completely distorted due to corrosion effects followed by simple diffusion of liquid $NaVO_3$, which was formed at 873 K from the above combination. Similarly at 1350 K, the corroded surface of the reaction zone appears with the combination of equiaxed and flake like structured corrosive grains. The EDX spectrum shown in Fig. 17 reveals the difference between these structures. It is seen from the figure that the equiaxed grains contain reaction products of both $LaVO_4$ and a significant quantity of ZrO_2. On the contrary, the flake like structure predominantly contains $LaVO_4$ and a very small quantity of ZrO_2. These results signify that the amount of ZrO_2 makes a difference in $LaVO_4$ crystallization. Well crystallized $LaVO_4$ has uneven morphology and its length varies from 10 to 20 µm. Furthermore, this new kind of corrosive product formation causes significant changes in the PRZ and MIRZ microstructure formation. A typical PRZ structure appears with cracks and some of the vertical cracks penetrated in MIRZ also. Thus, MIRZ appears as a PRZ embedded matrix microstructure as shown in Fig. 18. Formation and propagation of these cracks from the result of chemical interaction between the $La_2Zr_2O_7$ and molten mixture of $Na_2SO_4 + V_2O_5$ is the important factor resulting in degradation of the coating. According to the Lewis acid–base mechanism, metal oxides with the strongest basicity will react most severely with the highly acidic V_2O_5.[15] Moreover, the basicity of La_2O_3 is relatively higher than ZrO_2 in $La_2Zr_2O_7$ and it will react severely with the highly molten mixture of $Na_2SO_4 + V_2O_5$. Recently, similar kind of severe cracking and delamination was reported by Xu et al.[17] for their 3 wt.% Y_2O_3 added $La_2Zr_2O_7$ coating when it came into

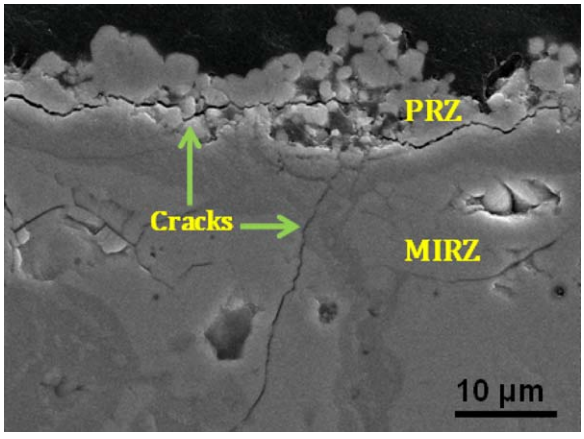

Fig. 18. Cross-sectional micrograph of $Na_2SO_4 + V_2O_5$ mixture reacted $La_2Zr_2O_7$ coating zone heat treated at 1350 K for 5 h.

contact with molten mixture of $Na_2SO_4 + V_2O_5$. The above coating was prepared by EB-PVD technique and is relatively resistant to attack from V_2O_5.

4. Summary and conclusions

Gas tunnel type plasma sprayed free-standing $La_2Zr_2O_7$ coating specimens with a thickness of about 300–400 μm were prepared under optimized operating conditions and characterized. The coatings retain the pyrochlore phase except for trivial losses of La_2O_3 and the coatings reflect the unique plasma spraying microstructure, i.e. lamella structures with pores. Furthermore, the coating specimens were subjected to hot corrosion testing in the presence of corrosive impurities such as V_2O_5, Na_2SO_4, and $Na_2SO_4 + V_2O_5$ mixtures (60:40, wt%) at two different temperatures for a duration of 5 h, i.e. 1000 and 1350 K for V_2O_5 and $Na_2SO_4 + V_2O_5$ mixtures, 1200 and 1350 K for Na_2SO_4.

After the hot corrosion testing against V_2O_5, depending on the temperature, two different reaction mechanisms were observed from the $La_2Zr_2O_7$ coating. The formation of ZrV_2O_7 was observed to be the predominant reaction rather than $LaVO_4$ at 1000 K. For temperatures at 1350 K, V_2O_5 reacts with La_2O_3 in $La_2Zr_2O_7$ to form $LaVO_4$ as the corrosive product and this leads to massive phase transformations from pyrochlore to tetragonal and monoclinic phases. Similarly, two different morphologies could be clearly identified from the cross-sectional views of V_2O_5 reacted $La_2Zr_2O_7$ coatings that correspond to a planar reacted zone (PRZ) and a melt infiltrated reaction zone (MIRZ). The morphology of the PRZ was mainly composed of clusters of sub-micron equiaxed particles such as ZrO_2, $LaVO_4$, and or ZrV_2O_7, and is almost similar at both temperatures. The MIRZ appeared as a dense infiltrated region with the lamella structure still evident, although the pores and cracks were filled with reaction products as in PRZ.

Hot corrosion test results against Na_2SO_4 showed that molten sodium sulfate is chemically inert in $La_2Zr_2O_7$ coating up to 1200 K. At 1350 K, it reacts with La_2O_3 to form lanthanum oxide sulfate, $La_2O_2SO_4$ as a corrosion product. Furthermore, it infiltrates into the interlamellar gaps and pores of $La_2Zr_2O_7$ coating and crystallizes while cooling, thus causing severe thermo-mechanical damage in both PRZ and MIRZ microstructures.

At the temperature range of 773 to 883 K, sodium metavanadate ($NaVO_3$) the major reaction product arising from the reaction of $Na_2SO_4 + V_2O_5$ mixture and the molten $NaVO_3$ continues to react with $La_2Zr_2O_7$ coating to form $LaVO_4$ as the final corrosion product at both temperatures, i.e. 1000 and 1350 K. The reaction mechanism showed $LaVO_4$ formation without ZrV_2O_7, similar to that for $La_2Zr_2O_7$–V_2O_5 at 1350 K. Thus, cross-sectional morphologies also appear to be similar to that of V_2O_5 reacted $La_2Zr_2O_7$ coating microstructure except for the existence of few cracks in PRZ and MIRZ.

From the aspect of microstructural observations, the present $La_2Zr_2O_7$ coating serves as an appropriate thermal barrier material in V_2O_5 environment. On the contrary, in Na_2SO_4 environment at high temperatures, the $La_2Zr_2O_7$ coatings fail to function as an effective thermal barrier material. Meanwhile, in $Na_2SO_4 + V_2O_5$ corrosive environment at elevated temperatures it performs moderately.

Acknowledgments

The authors would like to express their sincere gratitude to the Japan Society for the Promotion of Science (JSPS) for providing the financial support under the grant No. 21.09299 to conduct this research work. The support provided by Mr. T. Horinouchi during the plasma spraying and sample preparation is also gratefully acknowledged.

References

1. Miller RA. Current status of thermal barrier coatings. *Surf Coat Technol* 1987;**30**(1):1–11.
2. Beardsley MB. Thick thermal barrier coatings for diesel engines. *J Therm Spray Technol* 1997;**6**(2):181–6.
3. Vassen R, Stuke A, Stöver D. Recent developments in the field of thermal barrier coatings. *J Therm Spray Technol* 2009;**18**(2):181–6.
4. Vaßen R, Jarligo MO, Steinke T, Mack DE, Stöver D. Overview on advanced thermal barrier coatings. *Surf Coat Technol* 2010;**205**:938–42.
5. Saruhan B, Francois P, Fritscher K, Schulz U. EB-PVD processing of pyrochlore-structured $La_2Zr_2O_7$ based TBCs. *Surf Coat Technol* 2004;**182**:175–83.
6. Vassen R, Cao XQ, Tietz F, Kerkhoff G, Stöver D. *Proceedings of the United Thermal Spray Conference* 1999;**99**:830.
7. Subramanian MA, Aravamudan G, Subba Rao GV. Oxide pyrochlores: a review. *Prog Solid State Chem* 1983;**15**:55–143.
8. Vaßen R, Traeger F, Stöver D. New thermal barrier coatings based on pyrochlore/YSZ double-layer systems. *Int Appl Ceram Technol* 2004;**1**:351–61.
9. Cao XQ, Vassen R, Schwartz S, Jungen W, Tietz F, Stöver D. Spray-drying of ceramics for plasma-spray coating. *J Eur Ceram Soc* 2000;**20**:2433–9.
10. Vassen R, Cao X, Tietz F, Basu, Stöver D. Zirconates as new materials for thermal barrier coatings. *J Am Ceram Soc* 1999;**83**(8):2023–8.
11. Vaßen R, Pracht G, Stöver D. New thermal barrier coating systems with a graded ceramic coating. In: *Proc. of the International Thermal Spray Conference 2002*. 2001. pp. 202–207.
12. Vaßen R, Giesen S, Stoever D. Lifetime of plasma-sprayed thermal barrier coatings: comparison of numerical and experimental results. *J Therm Spray Technol* 2009;**18**:5–6. pp. 835–845.
13. Chen H, Liu Y, Gao Y, Tao S, Luo H. Design, preparation, and characterization of graded YSZ/$La_2Zr_2O_7$ thermal barrier coatings. *J Am Ceram Soc* 2010;**93**(6):1732–40.
14. Chen H, Liu Y, Gao Y, Tao S, Liu Y, Luo H. Thermophysical properties of lanthanum zirconate coating prepared by plasma spraying and the influence of post-annealing. *J Alloys Compd* 2009;**486**:391–9.
15. Chen Z, Speakman S, Howe J, Wang H, Porter W, Trice R. Investigation of reactions between vanadium oxide and plasma-sprayed yttria-stabilized zirconia coatings. *J Eur Ceram Soc* 2009;**29**:1403–11.
16. Marple BR, Voyer J, Thibodeau M, Nagy DR, Vassen R. Hot Corrosion of lanthanum zirconate and partially stabilized zirconia thermal barrier coatings. *J Eng Gas Turb Power* 2006;**128**:144–52.
17. Xu Z, He L, Mu R, He S, Huang G, Cao X. Hot corrosion behavior of $La_2Zr_2O_7$ with the addition of Y_2O_3 thermal barrier coatings in contacts with vanadate–sulfate salts. *J Alloys Compd* 2010;**504**(2):382–5.
18. Hamilton JC, Nagelberg AS. In-situ Raman spectroscopic study of yttria-stabilized zirconia attack by molten sodium vanadate. *J Am Ceram Soc* 1984;**67**(10):686–90.
19. Borom MP, Johnson CA, Peluso LA. Role of environmental deposits and operating surface temperature in spallation of air plasma sprayed thermal barrier coatings. *Surf Coat Technol* 1996;**8**:6–87, 116–126.
20. Jones RL. Thermal barrier coatings. In: Stern KH, editor. *Metallurgical and Ceramic Protective Coatings*. London: Chapman & Hall; 1996, p194-235.

21. Yoshiaki A, Kobayashi A. Application of a gas tunnel to high energy density plasma beams. *Appl Phys* 1986;**59**:3038–45.
22. Yoshiaki A, Kobayashi A, Habara Y. Ceramic coatings produced by means of a gas tunnel type plasma jet. *J Appl Phys* 1987;**62**:4884–90.
23. Kobayashi Akira. Formation of high hardness zirconia coatings by gas tunnel type plasma spraying. *Surf Coat Technol* 1997;**90**(3):197–202.
24. Yugeswaran S, Kobayashi A, Ananthapadmanabhan PV, Lusvarghi L. Influence of processing variables on the formation of $La_2Zr_2O_7$ in transferred arc plasma torch processing. *Curr App Phys* 2011;**11**(6):1394–400.
25. Xu Z, Zhong X, Zhang J, Zhang Y, Cao X, He L. Effects of deposition conditions on composition and thermal cycling life of lanthanum zirconate coatings. *Surf Coat Technol* 2008;**202**:4714–20.
26. Pannetier J. Energie electrostatique des reseaux pyrochlore. *J Phys Chem Solids* 1973;**34**:583–9.
27. Jones RL, Williams CE. Hot corrosion studies of zirconia ceramics. *Surf Coat Technol* 1987;**32**:349–58.
28. Reser MK. *Phase Diagrams for Ceramists—1969*. Columbus, OH: The American Ceramic Society; 1969.
29. Kamada T, Naoto W, Takashi M, Keiji D, Toshitaka O, Yasuo H. Synthesis and property of monazite type $LaVO_4$. *Rare Earths* 2002;**40**:120–1.
30. Chen Z, Mabon J, Wen J-G, Trice R. Degradation of plasma-sprayed yttria-stabilized zirconia coatings via ingress of vanadium oxide. *J Eur Ceram Soc* 2009;**29**:1647–56.
31. Szekely J, Evans JW. A structural model for gas-solid reactions with a moving boundary-II: the effect of grain size, porosity and temperature on the reaction of porous pellets. *Chem Eng Sci* 1971;**26**:1901–13.
32. Sohn HY, Szekely J. A structural model for gas-solid reactions with a moving boundary-III: a general dimensionless representation of the irreversible reaction between a porous solid and a reactant gas. *Chem Eng Sci* 1972;**27**:763–78.
33. Poston Jr JA, Siriwardane RV, Fisher EP, Miltz AL. Thermal decomposition of the rare earth sulfates of Cerium(III), Cerium(IV), Lanthanum(III), and Samarium(III). *Appl Surf Sci* 2003;**214**:83–102.
34. Nathans MW, Wendlandt WW. The thermal decomposition of the rare earth sulphates: thermogravimetric and differential thermal analysis studies up to 1400 °C. *J Inorg Nucl Chem* 1962;**24**:869–79.
35. Prabhakar Mohan, Yuan B, Patterson T, Desai VH, Yongho HS. Degradation of yttria stabilized zirconia thermal barrier coatings by vanadium pentoxide, phosphorous pentoxide, and sodium sulfate. *J Am Ceram Soc* 2007;**90**(11):601–3607.